inorganics

Article

A Robust Pyridyl-NHC-Ligated Rhenium Photocatalyst for CO_2 Reduction in the Presence of Water and Oxygen

Casey A. Carpenter, Phillip Brogdon, Louis E. McNamara, Gregory S. Tschumper, Nathan I. Hammer and Jared H. Delcamp *

Department of Chemistry and Biochemistry, University of Mississippi, 322 Coulter Hall, University, MS 38677, USA; carpe574@umn.edu (C.A.C.); pbrogdon@go.olemiss.edu (P.B.); lemcnama@go.olemiss.edu (L.E.M.); tschumpr@olemiss.edu (G.S.T.); nhammer@olemiss.edu (N.I.H.)

*** Correspondence: delcamp@olemiss.edu; Tel.: +1-662-915-5332**

Received: 2 January 2018; Accepted: 22 January 2018; Published: 25 January 2018

Abstract: $Re(pyNHC\text{-}PhCF_3)(CO)_3Br$ is a highly active photocatalyst for CO_2 reduction. The $PhCF_3$ derivative was previously empirically shown to be a robust catalyst. Here, the role of the $PhCF_3$ group is probed computationally and the robust nature of this catalyst is analyzed with regard to the presence of water and oxygen introduced in controlled amounts during the photocatalytic reduction of CO_2 to CO with visible light. This complex was found to work well from 0–1% water concentration reproducibly; however, trace amounts of water were required for benchmark $Re(bpy)(CO)_3Cl$ to give reproducible reactivity. When ambient air is added to the reaction mixture, the NHC complex was found to retain substantial performance (~50% of optimized reactivity) at up to 40% ambient atmosphere and 60% CO_2 while the $Re(bpy)(CO)_3Cl$ complex was found to give a dramatically reduced CO_2 reduction reactivity upon introduction of ambient atmosphere. Through the use of time-correlated single photon counting studies and prior electrochemical results, we reasoned that this enhanced catalyst resilience is due to a mechanistic difference between the NHC- and bpy-based catalysts. These results highlight an important feature of this NHC-ligated catalyst: substantially enhanced stability toward common reaction contaminates.

Keywords: CO_2 reduction; photocatalysis; NHC-ligated complexes

1. Introduction

The photocatalytic transformation of CO_2 into a useful fuel is one of humanity's paramount challenges [1–4]. Driving this process with widely abundant sunlight is highly desirable. The use of a catalyst to drive the multi-electron reduction of CO_2 is needed as the direct one-electron reduction is energetically inhibitive [5,6]. Thus, catalysts that can absorb sunlight and deliver multiple electrons simultaneously are in high demand for addressing two key challenges. Despite more than 30 years of exploration, very few catalysts meet these criteria with a single metal center, and nearly all of them are based on one of five frameworks: Fe-p-TMA, Ir(tpy)(ppy)X, Ir(tpy)(bpy)X, $Re(bpy)(CO)_3X$, or $Re(pyNHC\text{-}R)(CO)_3X$ (Figure 1) [7–12]. Among these catalysts, the $Re(pyNHC\text{-}R)(CO)_3X$ catalyst is unique in allowing the reduction of CO_2 to occur at the first reduction potential of the neutral catalyst (Figure 2) [10,13]. Typically, CO_2 reduction photocatalysts first undergo photoexcitation followed by electron transfer from a sacrificial electron donor (SED) to give the anionic catalyst (Figure 2a). An SED is used in place of a complete photoelectrochemical system to reduce complexity and allow for the study of a single catalyst. The anionic complex then receives a second electron ultimately from a SED. The catalyst can then reduce CO_2 to a lower-oxidation-state carbon-based product such as CO and regenerate the initial neutral catalyst. Alternatively, after the first reduction sequence, the catalyst can

can then reduce CO_2 to a lower-oxidation-state carbon-based product such as CO and regenerate the initial neutral catalyst. Alternatively, after the first reduction sequence, the catalyst can attack CO$_2$ before the second reduction event (Figure 2b). Catalysis occurring after the first reduction is a property that is commonly observed for NHC catalysts and rarely observed for pyridyl-based systems [10,14–19]. Reactions operating off the first reduction potential for activation of CO$_2$ can be beneficial in designing catalysts with lower overpotentials (the excess energy beyond what is needed to reduce CO_2) which will be important in complete photoelectrochemical systems. In these systems, the energetics of the active catalyst which attacks CO$_2$ are readily measured and can be rationally tuned [18].

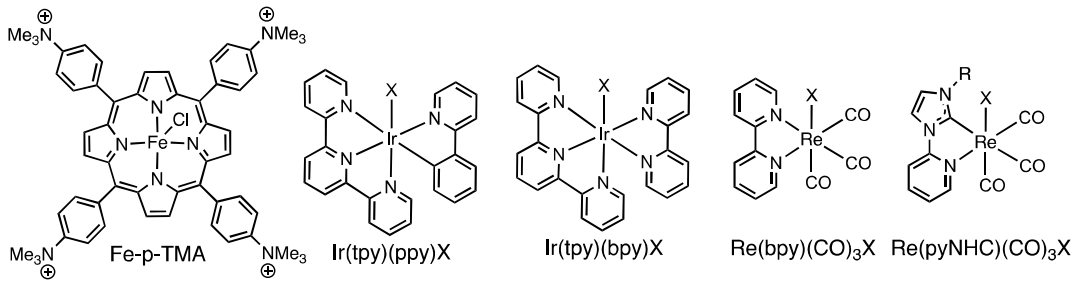

Figure 1. Known photocatalysts for CO_2 reduction.

In addition to a key mechanistic difference during photocatalytic CO_2 reduction reactions, NHC-ligated catalysts have long been heralded as robust, highly reactive systems in general [20–23]. Concerning photocatalytic CO_2 reduction with sunlight, only one catalyst framework has been put forward utilizing an NHC ligand [10]. Interestingly, when an electron-deficient aryl-CF_3 group was used at the NHC wingtip, the catalyst was found to be faster reacting and more durable than Lehn's bipyridyl analogue under anhydrous conditions (Figure 2). In this study, we probe the role of the critical-to-reactivity CF_3 group computationally and compare the properties of the two catalysts through excited-state lifetime measurements. Additionally, we evaluate the resilience of each catalyst to common reaction contaminates such as water and ambient atmosphere (O_2).

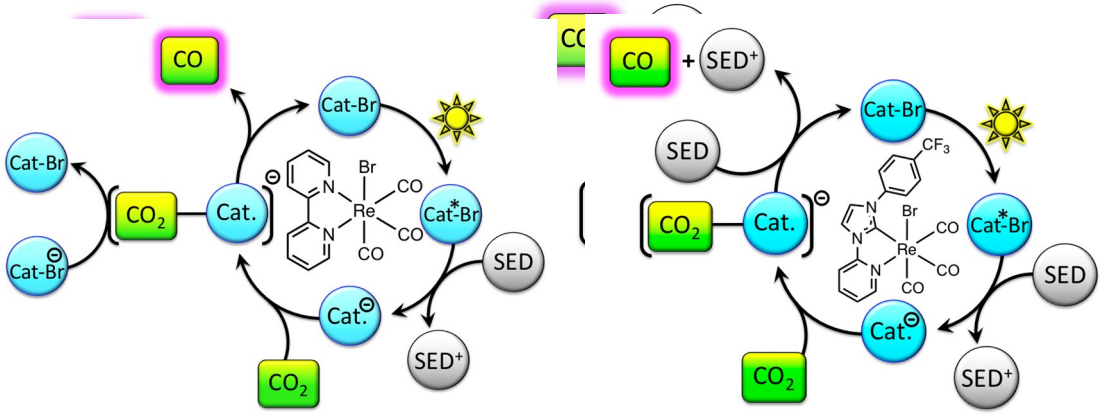

Figure 2. Generic catalytic cycles for catalysts that reduce CO_2 after (**a**) the second catalyst reduction event, such as benchmark bpy-based Re(bpy)(CO)$_3$Br, or (**b**) the first catalyst reduction event, such as NHC-based Re(pyNHC-PhCF$_3$)(CO)$_3$Br. Note: The first reduction event is drawn as two steps (photoexcitation and electron transfer) to aid in discussion, while the second reduction event combines these steps.

In addition to a key mechanistic difference during photocatalytic CO$_2$ reduction reactions, NHC-ligated catalysts have long been heralded as robust, highly reactive systems in general [20–23]. Concerning photocatalytic CO$_2$ reduction with sunlight, only one catalyst framework has been put forward utilizing an NHC ligand [10]. Interestingly, when an electron-deficient aryl-CF$_3$ group was used at the NHC wingtip, the catalyst was found to be faster reacting and more durable than Lehn's bipyridyl analogue under anhydrous conditions (Figure 2). In this study, we probe the role of the critical-to-reactivity CF$_3$ group computationally and compare the properties of the two catalysts through excited-state lifetime measurements. Additionally, we evaluate the resilience of each catalyst to common reaction contaminates such as water and ambient atmosphere (O$_2$).

Figure 2. Generic catalytic cycles for catalysts that reduce CO$_2$ after (**a**) the second catalyst reduction event, such as benchmark bpy-based Re(bpy)(CO)$_3$Br, or (**b**) the first catalyst reduction event, such as NHC-based Re(pyNHC-PhCF$_3$)(CO)$_3$Br. Note: The first reduction event is drawn as two steps (photoexcitation and electron transfer) to aid in discussion, while the second reduction event combines these steps. Br atom transfers are understood, and the mechanism in (**a**) is provided via analogy to a prior study [24]. Additional photoexcitations may be needed but are not specifically drawn.

2. Results and Discussion

2.1. Computational Analysis: Role of the Ph-CF_3 Substituent

Among known NHC-ligated photocatalysts, the phenyl-CF_3 substituent was previously found to give the most reactive catalyst when compared with phenyl, hexyloxyphenyl, or methyl substituents on the NHC ring [10]. Here, we have used computational analysis to better delocalization of the added electron on the singly reduced catalyst across the ligand framework since the lowest energy excitation is thought to be a metal-to-ligand charge transfer (MLCT) followed by addition of an electron [25–27]. To analyze the role of the phenyl-CF_3 substituent, the geometry of Re(pyNHC-PhCF$_3$)(CO)$_3$Br was first optimized with DFT at the M06-L/6-311+G(*d*,*p*) level. Analysis of the highest occupied molecular orbital (HOMO) distribution (HOMO, Figure 3a) shows the orbital primarily situated on the Re metal center, the CO ligands, and the Br ligand with no contribution from the pyNHC-PhCF$_3$ ligand (Figure 3a). The lowest unoccupied molecular orbital (LUMO) distribution (LUMO, Figure 3b) is primarily located on the pyridyl and NHC rings of the pyNHC-PhCF$_3$ ligand, which confirms the presence of an MLCT event. Interestingly, the PhCF$_3$ group has a dihedral angle (~50°) relative to the NHC ring. This angle is large enough to inhibit contribution of the PhCF$_3$ group to the LUMO. This explains the observation that the NHC group substituent has only a minor role in controlling catalyst reduction potentials, but the origin of the increased reducibility of the CF$_3$ complex is both of the CF$_3$ HOMO/LUMO orbital images. However, Lutterman et al. previously computationally analyzed the singly reduced catalyst species and found substantial involvement of the phenyl-CF$_3$ group in the single occupied molecular orbital (SOMO) distribution. In addition to the HOMO distribution from the phenyl-CF$_3$ group to the SOMO, the phenyl-CF$_3$ group twist angle is dramatically reduced (from ~50° to ~35°). This observation suggests that the primary contribution of the phenyl-CF$_3$ group is to stabilize the highly reactive reduced catalyst. Presumably, this stability preserves more active catalyst in solution leading to a more durable catalyst (higher turnover number (TON)) compared to other NHC photocatalysts.

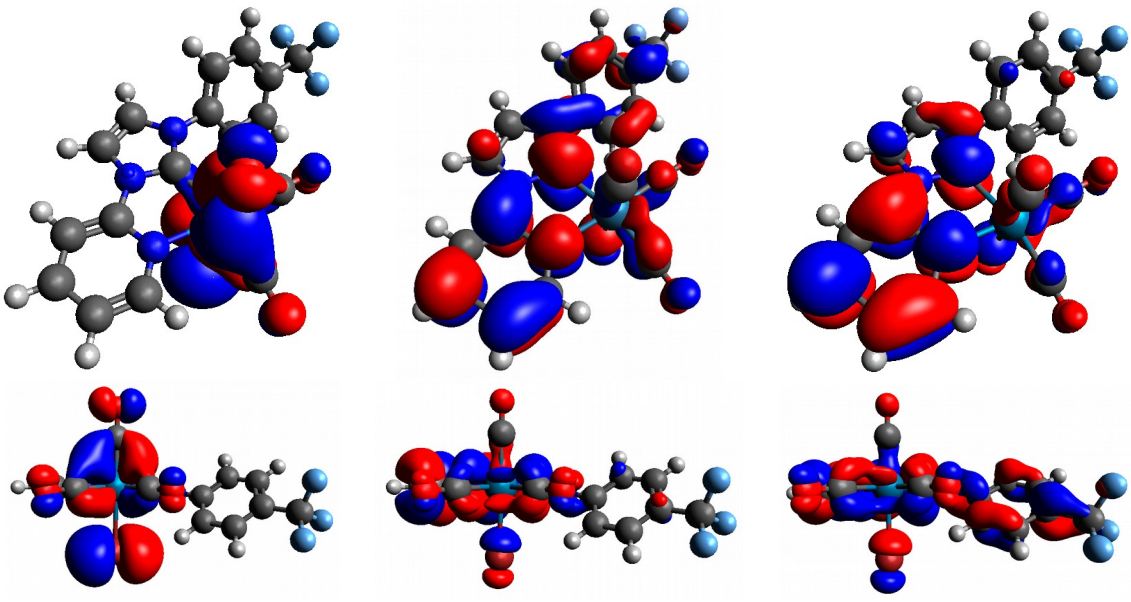

(**a**) (**b**) (**c**)

Figure 3. Re(pyNHC-PhCF$_3$)(CO)$_3$Br (**a**) HOMO, (**b**) LUMO and (**c**) single occupied molecular orbital (SOMO) images. Top row shows the ligand π-face primarily, and the second row shows the Re centered with the ligand on edge in back.

The computational results also aid in understanding the unique irreversibility of the NHC catalysts toward single-electron reduction when compared with the reversible first reduction of Re(bpy)(CO)$_3$Br [10]. The Re–Br bond was found to substantially lengthen upon reduction by 0.08 Å when the neutral catalyst is compared with the singly reduced catalyst. The remaining Re–ligand

Re(bpy)(CO)$_3$Br [10]. The Re–Br bond was found to substantially lengthen upon reduction by 0.08 Å when the neutral catalyst is compared with the singly reduced catalyst.The remaining Re–ligand bonds change a relatively minor amount with the Re–CO and Re–N bonds slightly shortening and the Re–NHC bond slightly increasing in length by ≤0.03 Å. This suggests that the irreversible event occurring upon the first reduction of Re(pyNHC-PhCF$_3$)(CO)$_3$Br is the loss of Br. The increased lability of this halide is potentially affected by the electron-rich nature of the NHC ring both increasing electron density at the Re center and weakly (relative to a pyridyl) stabilizing the ligand centered anion of the reduced complex. This increased electron density at the Re metal center likely leads to the lengthening of the Re–Br bond to give a more facile dissociation of the anionic bromide atom. The Br dissociated complex is known to react with CO$_2$ after the first reduction of Re(pyNHC-PhCF$_3$)(CO)$_3$Br, and this reduction/dissociation is a key step in accessing the active catalytic intermediate earlier in the catalytic cycle for NHC-based catalysts. It is apparent that the NHC ligand plays a key role in controlling the photoexcitation energy and electron storage after reduction, and likely indirectly aids in halide dissociation. Further studies are needed to better understand the role of the NHC ligand relative to bpy ligands.

bonds change a relatively minor amount with the Re–CO and Re–N bonds slightly shortening and the Re–NHC bond slightly increasing in length by ≤0.03 Å. This suggests that the irreversible event occurring upon the first reduction of Re(pyNHC-PhCF$_3$)(CO)$_3$Br is the loss of Br. The increased lability of this halide is potentially affected by the electron-rich nature of the NHC ring both increasing electron density at the Re center and weakly (relative to a pyridyl) stabilizing the ligand centered anion of the reduced complex. This increased electron density at the Re metal center likely leads to the lengthening of the Re–Br bond to give a more facile dissociation of the anionic bromide atom. The Br dissociated complex is known to react with CO$_2$ after the first reduction of Re(pyNHC-PhCF$_3$)(CO)$_3$Br, and this reduction/dissociation is a key step in accessing the active catalytic intermediate earlier in the catalytic cycle for NHC-based catalysts. It is apparent that the NHC ligand plays a key role in controlling the photoexcitation energy and electron storage after reduction, and likely indirectly aids in halide dissociation. Further studies are needed to better understand the role of the NHC ligand relative to bpy ligands.

2.2. Excited-State Lifetime: Mechanistic Implications

2.2. Excited-State Lifetime: Mechanistic Implications

Accessing a highly reactive catalyst intermediate after a single reduction is additionally beneficial when considering the excited-state lifetimes of Re(pyNHC-PhCF$_3$)(CO)$_3$Br versus Re(bpy)(CO)$_3$Br in acetonitrile. We have previously reported an enhanced reactivity of Re(pyNHC-PhCF$_3$)(CO)$_3$Br over Re(bpy)(CO)$_3$Br for the photocatalytic conversion of CO$_2$ to CO in terms both of rate and durability. The first step of the catalytic cycle for both of these catalysts is photoexcitation followed by reduction of the catalyst with an SED. Thus, the excited-state lifetimes of the complexes are an important factor in controlling the amount of reduced complex being generated in solution. Through the use of time-correlated single photon counting (TCSPC) measurements on the two catalysts, the excited-state lifetime was found to be 4.2 ns for Re(pyNHC-PhCF$_3$)(CO)$_3$Br and 150 ns for Re(bpy)(CO)$_3$Br in N$_2$ degassed acetonitrile (Figure 4).

Accessing a highly reactive catalyst intermediate after a single reduction is additionally beneficial when considering the excited-state lifetimes of ^{3}Re(pyNHC-PhCF$_3$)(CO)$_3$Br versus Re(bpy)(CO)$_3$Br in acetonitrile. We have previously reported an enhanced reactivity of Re(pyNHC-PhCF$_3$)(CO)$_3$Br over Re(bpy)(CO)$_3$Br for the photocatalytic conversion of CO$_2$ to CO in terms both of rate and durability. The first step of the catalytic cycle for both of these catalysts is photoexcitation followed by reduction of the catalyst with an SED. Thus, the excited-state lifetimes of the complexes are an important factor in controlling the amount of reduced complex being generated in solution. Through the use of time-correlated single photon counting (TCSPC) measurements on the two catalysts, the excited-state lifetime was found to be 4.2 ns for Re(pyNHC-PhCF$_3$)(CO)$_3$Br and 150 ns for Re(bpy)(CO)$_3$Br in N$_2$ degassed acetonitrile (Figure 4).

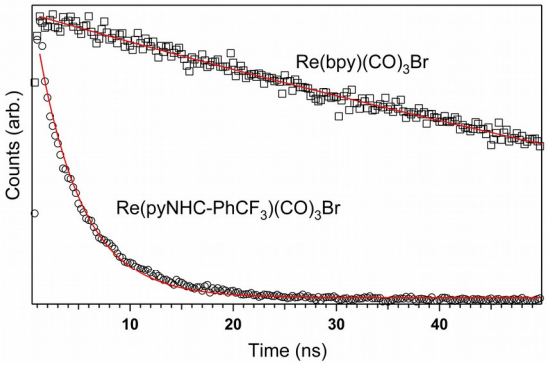

Figure 4. Time-correlated single photon counting (TCSPC) luminescence decays of Re(pyNHC-PhCF$_3$)(CO)$_3$Br and Re(bpy)(CO)$_3$Br.

Figure 4. Time-correlated single photon counting (TCSPC) fluorescence decays of Re(pyNHC-PhCF$_3$)(CO)$_3$Br and Re(bpy)(CO)$_3$Br.

The NHC ligand dramatically shortens the excited-state lifetime by 36 times when compared with the bipyridyl analogue. This decreased time scale, however, did not correlate to diminished reactivity which suggests that this catalyst is remarkably active toward CO$_2$ addition. Energetically, a slightly larger ΔG exists for the transfer of an electron from 1,3-dimethyl-2-phenyl-2,3-dihydro-1H-benzo[d]imidazole (BIH, the SED used in our study) to the Re(bpy)(CO)$_3$Br catalyst (1.03 V versus 1.14 V) [10]. The outer-sphere electron transfer from the SED to the photoexcited catalyst (cat*) is presumably governed by Markus theory kinetics, with the ΔG values not being large enough to typically lie conclusively within the inverted region [27,28]. Thus, a larger ΔG should correlate to a more facile electron transfer event. This suggests that a dramatically larger amount of reduced Re(bpy)(CO)$_3$Br is present in solution relative to reduced Re(pyNHC-PhCF$_3$)(CO)$_3$Br due to both a shorter excited-state lifetime for the NHC catalyst and a smaller ΔG for the electron transfer from BIH to the NHC catalyst. However, it is important to recall that the Re(pyNHC-PhCF$_3$)(CO)$_3$Br catalyst reacts CO$_2$ after a single electron transfer, which means that a CO$_2$ reactive species is being generated

The NHC ligand dramatically shortens the excited-state lifetime by 36 times when compared with the bipyridyl analogue. This decreased time scale, however, did not correlate to diminished reactivity which suggests that this catalyst is remarkably active toward CO$_2$ addition. Energetically, a slightly larger ΔG exists for the transfer of an electron from 1,3-dimethyl-2-phenyl-2,3-dihydro-1H-benzo[d]imidazole (BIH, the SED used in our study) to the Re(bpy)(CO)$_3$Br catalyst (1.03 V versus 1.14 V) [10]. The outer-sphere electron transfer from the SED to the photoexcited catalyst (cat*) is presumably governed by Markus theory kinetics, with the ΔG values not being large enough to typically lie conclusively within the inverted region [27,28]. Thus, a larger ΔG should correlate to a more facile electron transfer event. This suggests that a dramatically larger amount of reduced Re(bpy)(CO)$_3$Br is present in solution relative to reduced Re(pyNHC-PhCF$_3$)(CO)$_3$Br due to both a shorter excited-state lifetime for the NHC catalyst and a smaller ΔG for the electron transfer from BIH to the NHC catalyst. However, it is important to recall that the Re(pyNHC-PhCF$_3$)(CO)$_3$Br catalyst reacts CO$_2$ after a single electron transfer, which means that a CO$_2$ reactive species is being generated

a more facile electron transfer event. This suggests that a dramatically larger amount of reduced Re(bpy)(CO)$_3$Br is present in solution relative to reduced Re(pyNHC-PhCF$_3$)(CO)$_3$Br due to both a shorter excited-state lifetime for the NHC catalyst and a smaller ΔG for the electron transfer from BIH to the NHC catalyst. However, it is important to recall that the Re(pyNHC-PhCF$_3$)(CO)$_3$Br catalyst reacts CO_2 after a single electron transfer, which means that a CO_2-reactive species is being generated after a single photoexcitation and SED electron transfer. The reduced Re(bpy)(CO)$_3$Br catalyst likely undergoes a second electron transfer event before CO release. The relative concentration of the species being reduced is difficult to predict, although the singly reduced Re(bpy)(CO)$_3$Br will be lower in concentration than neutral Re(pyNHC-PhCF$_3$)(CO)$_3$Br, both of which require one electron transfer to become reactive toward CO_2 and produce CO. Thus, the higher reactivity of the Re(pyNHC-PhCF$_3$)(CO)$_3$Br catalyst (relative to Re(bpy)(CO)$_3$Br) toward photocatalytic CO_2 reduction could be due to a higher concentration of CO_2-reactive species in solution or due to a more reactive catalyst or both.

2.3. Catalyst Sensitivity: Water Concentration

We reasoned that the differences in mechanisms could lead to an NHC-ligated catalyst that is more robust to water and O_2. Initial anhydrous, O_2 free experiments reveal a closer match in TON values for the Re(bpy)(CO)$_3$Cl and Re(pyNHC-PhCF$_3$)(CO)$_3$Cl complexes (2–3 TON difference) than the Br derivatives (~15 TON difference). Thus, the Cl complexes were examined toward water and oxygen sensitivity from a common TON starting point. Both Re(pyNHC-PhCF$_3$)(CO)$_3$Cl and Re(bpy)(CO)$_3$Cl are stable to ambient air and moisture for prolonged periods with no noticeable loss of reactivity provided that light exposure is avoided. However, the anionic catalysts are presumably much more reactive toward water and oxygen. As a key difference in these catalysts, though, Re(bpy)(CO)$_3$Cl must access a doubly reduced species to be competent toward CO_2 reduction. Thus, the stability of both the first and second reduced catalyst species related to Re(bpy)(CO)$_3$Cl toward water and oxygen must be considered, while only the Re(pyNHC-PhCF$_3$)(CO)$_3$Cl anion needs to be considered due to the NHC ligand. This led us to hypothesize that the NHC catalyst would be more resilient to these common contaminates.

To probe this hypothesis, we compared the head-to-head photocatalytic reduction of CO_2 reactions with Re(pyNHC-PhCF$_3$)(CO)$_3$Cl and Re(bpy)(CO)$_3$Cl with controlled addition of water or ambient atmosphere to the reaction. We monitored the changes in rates of reactivity (turnover frequency, TOF) and the overall durability of the catalysts (turnover number, TON) for these comparisons. Concerning water, seven low-reaction solvent volume ratios were analyzed starting from dried and distilled anhydrous MeCN up to 3.2% water concentration. For the benchmark Re(bpy)(CO)$_3$Cl complex, strictly anhydrous conditions show a relatively low TON value (26) compared to the highest TON value of 72 with the addition of 0.05% water volume (Figure 5). This represents at least a 64% loss in reactivity relative to peak performance.

Interestingly, a near trace amount of water is needed to observe high reactivity with the Re(bpy)(CO)$_3$Cl catalyst, but addition of water beyond 0.05% leads to a slight decrease in durability up to 0.80% volume water before a large drop in reactivity is observed. It should be noted that the anhydrous TON value is reported as an average of several experiments with a very large variability in TON values between 62 and 4 TON (Figure 5c). We suspect that this catalyst requires a very small amount of water to perform the photocatalytic reduction of CO_2 and that the variability is due to trace amounts of adventitious water entering our reactions despite our attempts to run these reactions under strictly anhydrous conditions.

The Re(pyNHC-PhCF$_3$)(CO)$_3$Cl complex shows a similar trend with the anhydrous conditions giving about 20 TON and the peak catalyst performances observed with 0.20% water volume (35 TON, Figure 5b). While water does enhance the reactivity of Re(pyNHC-PhCF$_3$)(CO)$_3$Cl, the loss of reactivity (43%) under anhydrous conditions is much less than that of Re(bpy)(CO)$_3$Cl. Again, addition of larger amounts of water (up to 3.2%) shows a dramatic loss in catalyst reactivity. Interestingly,

the variation in catalyst performance of about +/ − 5 TON under anhydrous conditions with Re(pyNHC-PhCF$_3$)(CO)$_3$Cl is no larger than under peak performance conditions and compares favorably to the +/− 30 TON observed for Re(bpy)(CO)$_3$Cl under anhydrous conditions (Figure 5d). This observation helps to explain the wide range of TON values observed with Lehn's catalyst (Re(bpy)(CO)$_3$Cl) from various research groups under "anhydrous" conditions, since even rigorously anhydrous experimental technique results are substantially variable.

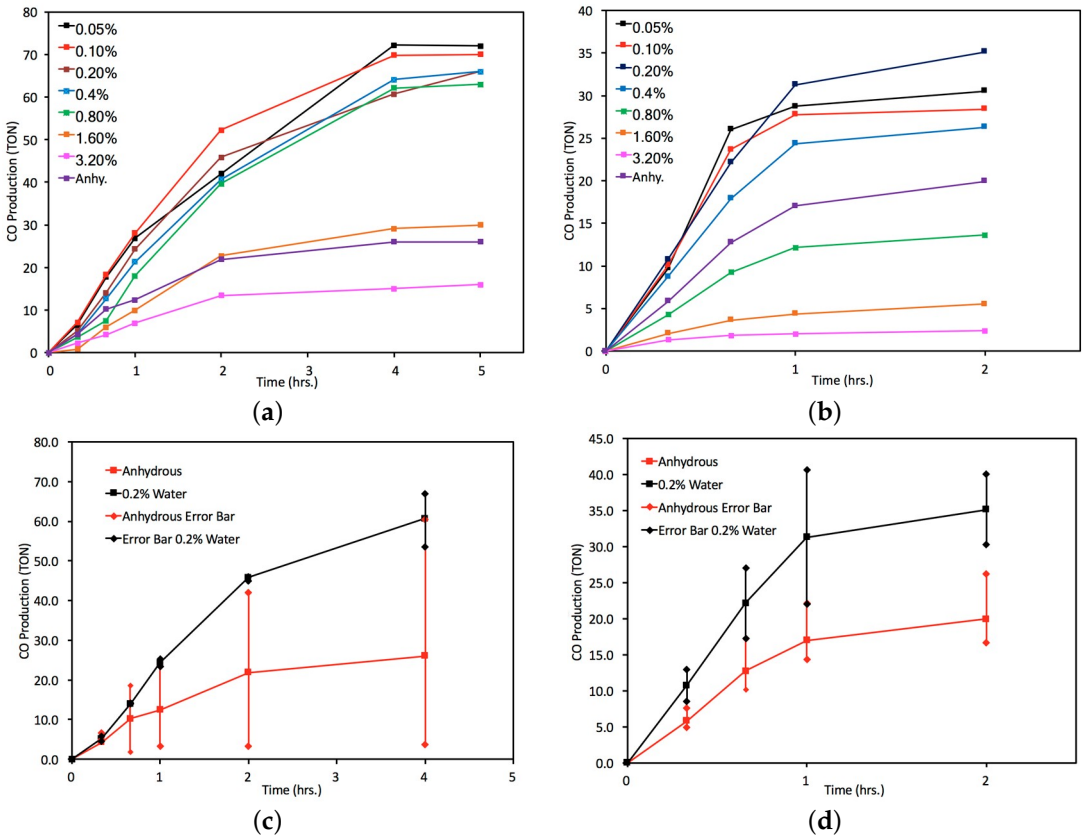

Figure 5. Turnover number (TON) values over time with varying water concentrations for (a) Re(bpy)(CO)$_3$Cl and (b) Re(pyNHC-PhCF$_3$)(CO)$_3$Cl. Variation in TON values over time under anhydrous or 0.2% water volume with high and low TON values shown as vertical bars for (c) Re(bpy)(CO)$_3$Cl and (d) Re(pyNHC-PhCF$_3$)(CO)$_3$Cl.

2.4. Catalyst Sensitivity: Air Concentration

Under practical conditions, CO_2 volumes may only make up 3% of the total gas present [28]. Thus, a catalyst which operates under reduced CO_2 concentrations is highly desirable [29]. To prove the reactivity of each catalyst with reduced CO_2 concentrations, ambient atmosphere (air) was added as the makeup gas. Through this study, we were able to evaluate the efficiency of these catalysts both under lowered substrate concentrations and toward resilience to O_2. Air was added in quantities ranging from 0 to 40% prior to initiating photocatalysis with 0.20% water present to ensure reproducible results for Re(bpy)(CO)$_3$Cl. Both catalysts work best with 0 added air (Figure 6).

However, the NHC catalyst only shows a 66% reduction in TON for all air concentrations from 1% to 40%. On the other hand, the bpy catalyst shows a continual loss of TON values as air in the reaction headspace increases to 40% for a 91% reduction in TON. Despite starting with a lower TON value at 0% air, the Re(pyNHC-PhCF$_3$)(CO)$_3$Cl catalyst outperforms Re(bpy)(CO)$_3$Cl at 20% air volume and higher due to no relative loss of reactivity under these conditions. This highlights the high relative stability of Re(pyNHC-PhCF$_3$)(CO)$_3$Cl to O_2, which is potentially due to the mechanistic differences in reactive anions present for the two catalysts, as described above. The TOF of these reactions was analyzed at the earliest time point to see the maximal TOF value under each air percentage. Re(pyNHC-PhCF$_3$)(CO)$_3$Cl is fastest with no air present (35 TON/h) while the Re(bpy)(CO)$_3$Cl catalyst is significantly slower at 16 TON/h (Figure 7). The Re(bpy)(CO)$_3$Cl catalyst gradually loses its initial TOF rate as more air is added. Surprisingly, after an initial loss of TOF as air increases, Re(pyNHC-PhCF$_3$)(CO)$_3$Cl shows an increase in TOF at air concentrations of 20% or

Under practical conditions, CO_2 volumes may only make up 3% of the total gas present in exhaust from fire power plants [29]. Thus, a catalyst which operates under reduced CO_2 concentrations is highly desirable [30]. To prove the reactivity of each catalyst with reduced CO_2 concentrations, ambient atmosphere (air) was added as the makeup gas. Through this study, we were able to evaluate the efficiency of these catalysts both under lowered substrate concentrations and toward resilience to O_2. Air was added in quantities ranging from 0 to 40% prior to initiating photocatalysis with 0.20% water present to ensure reproducible results for Re(bpy)(CO)$_3$Cl. Both catalysts work best with 0 added air (Figure 6).

However, the NHC catalyst only shows a 66% reduction in TON for all air concentrations from 1% to 40%. On the other hand, the bpy catalyst shows a continual loss of TON values as air in the reaction headspace increases to 40% for a 91% reduction in TON. Despite starting with a lower TON value at 0% air, the Re(pyNHC-PhCF$_3$)(CO)$_3$Cl catalyst outperforms Re(bpy)(CO)$_3$Cl at 20% air volume and higher due to no relative loss of reactivity under these conditions. This highlights the high relative

stability of Re(pyNHC-PhCF$_3$)(CO)$_3$Cl to O$_2$, which is potentially due to the mechanistic differences in reactive anions present for the two catalysts, as described above. The TOF of these reactions was analyzed at the earliest time point to see the maximal TOF value under each air percentage. Re(pyNHC-PhCF$_3$)(CO)$_3$Cl is fastest with no air present (35 TON/h) while the Re(bpy)(CO)$_3$Cl catalyst is significantly slower at 16 TON/h (Figure 7). The Re(bpy)(CO)$_3$Cl catalyst gradually loses its initial TOF rate as more air is added. Surprisingly, after an initial loss of TOF as air increases, Re(pyNHC-PhCF$_3$)(CO)$_3$Cl shows an increase in TOF at air concentrations of 20% or more. This effect is even more dramatic if the TOF is normalized to the percent of CO$_2$ present in the reaction vessel. In this case, at 40% air, Re(pyNHC-PhCF$_3$)(CO)$_3$Cl is as fast as with 0% air with a gradual loss of TOF at intermediate air volumes. The origin of this increase in TOF and the rationale for such a high stability of Re(pyNHC-PhCF$_3$)(CO)$_3$Cl toward O$_2$ is not apparent. However, we can conclude that Re(pyNHC-PhCF$_3$)(CO)$_3$Cl is significantly more robust to O$_2$ than Re(bpy)(CO)$_3$Cl.

Inorganics **2018**, *6*, x FOR PEER REVIEW **7 of 11**

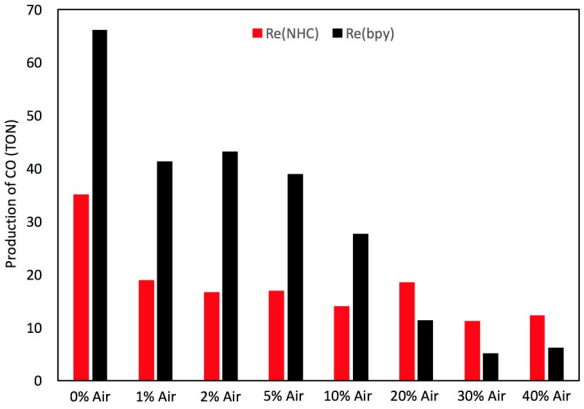

Figure 6. Maximum TON values for Re(pyNHC-PhCF$_3$)(CO)$_3$Cl and Re(bpy)(CO)$_3$Cl with varying percentages of air.

Figure 6. Maximum TON values for Re(pyNHC-PhCF$_3$)(CO)$_3$Cl and Re(bpy)(CO)$_3$Cl with varying percentages of air.

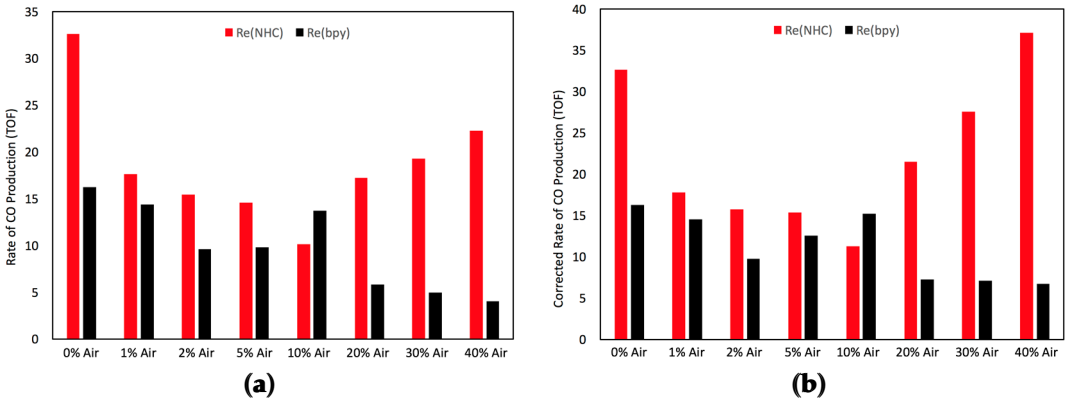

Figure 7. Maximum turnover frequency (TOF) values for Re(pyNHC-PhCF$_3$)(CO)$_3$Cl and Re(bpy)(CO)$_3$Cl with varying percentages of air (**a**) without normalization and (**b**) with normalization to percentage of CO$_2$ present.

Figure 7. Maximum turnover frequency (TOF) values for Re(pyNHC-PhCF$_3$)(CO)$_3$Cl and Re(bpy)(CO)$_3$Cl with varying percentages of air (**a**) without normalization and (**b**) with normalization to percentage of CO$_2$ present.

In conclusion, the NHC-based ligand on Re(pyNHC-PhCF$_3$)(CO)$_3$Br was shown to have SOMO delocalization onto the PhCF$_3$ ring after the catalyst was reduced with a planarization of the ligand π-system. This result illustrates the importance of substituent selection for the NHC wingtip. Through time-correlated single photon counting studies, the Re(pyNHC-PhCF$_3$)(CO)$_3$Br complex was found to have a dramatically shorter excited-state lifetime than the benchmark Re(bpy)(CO)$_3$Br complex. Presumably due to a difference in catalyst mechanisms, Re(pyNHC-PhCF$_3$)(CO)$_3$Cl maintains comparable or higher reactivity than Re(bpy)(CO)$_3$Cl for the photocatalytic reduction of CO$_2$ despite the tremendously shortened excited state. Concerning common contaminates, added water was found to be critical for reproducible reactivity with Re(bpy)(CO)$_3$Cl while Re(pyNHC-PhCF$_3$)(CO)$_3$Cl was significantly less sensitive to anhydrous conditions. Both catalysts show substantially reduced reactivity when water reached ~1% of the solvent volume. With regard to reduced CO$_2$ concentration with O$_2$ incorporation from ambient atmosphere as the makeup gas, Re(pyNHC-PhCF$_3$)(CO)$_3$Cl was found to be significantly less sensitive than Re(bpy)(CO)$_3$Cl as

In conclusion, the NHC-based ligand on Re(pyNHC-PhCF$_3$)(CO)$_3$Br was shown to have SOMO delocalization onto the PhCF$_3$ ring after the catalyst was reduced with a planarization of the ligand π-system. This result illustrates the importance of substituent selection for the NHC wingtip. Through time-correlated single photon counting studies, the Re(pyNHC-PhCF$_3$)(CO)$_3$Br complex was found to have a dramatically shorter excited-state lifetime than the benchmark Re(bpy)(CO)$_3$Br complex. Presumably due to a difference in catalyst mechanisms, Re(pyNHC-PhCF$_3$)(CO)$_3$Cl maintains comparable or higher reactivity than Re(bpy)(CO)$_3$Cl for the photocatalytic reduction of CO$_2$ despite the tremendously shortened excited state. Concerning common contaminates, added water was found to be critical for reproducible reactivity with Re(bpy)(CO)$_3$Cl while Re(pyNHC-PhCF$_3$)(CO)$_3$Cl was significantly less sensitive to anhydrous conditions. Both catalysts show substantially reduced reactivity when water reached ~1% of the solvent volume. With regard to reduced CO$_2$ concentration with O$_2$ incorporation from ambient atmosphere as the makeup gas, Re(pyNHC-PhCF$_3$)(CO)$_3$Cl was found to be significantly less sensitive than Re(bpy)(CO)$_3$Cl as

the tremendously shortened excited state. Concerning common contaminates, added water was found to be critical for reproducible reactivity with Re(bpy)(CO)$_3$Cl while Re(pyNHC-PhCF$_3$)(CO)$_3$Cl was significantly less sensitive to anhydrous conditions. Both catalysts show substantially reduced reactivity when water reached ~1% of the solvent volume. With regard to reduced CO$_2$ concentration with O$_2$ incorporation from ambient atmosphere as the makeup gas, Re(pyNHC-PhCF$_3$)(CO)$_3$Cl was found to be significantly less sensitive than Re(bpy)(CO)$_3$Cl as ambient atmosphere concentrations increased. Interestingly, Re(pyNHC-PhCF$_3$)(CO)$_3$Cl was found to have a similar turnover frequency at 0% ambient atmosphere (100% CO$_2$) as at 40% ambient atmosphere once the amount of CO$_2$ was normalized. Future studies will focus on the examination of NHC ligand designs to find a more durable catalyst given the unique properties of NHC-ligated complexes in photocatalytic CO$_2$ reduction reactions. Additionally, we plan to evaluate new metal centers with future ligand designs as the combined role that the ligand and metal center play in CO$_2$ reduction is likely important but not fully understood.

3. Experimental Section

3.1. Computational Details

Density functional theory (DFT) was used to compute the optimized structures and harmonic vibrational frequencies for both the neutral (18 e^-) and anionic (19 e^-) systems. The M06-L [31] functional was employed for these computations. The density fitting approximation was employed with M06-L using the default auxiliary basis sets in the Gaussian 09 (Rev: E.01) software package [32]. The Hay–Wadt relativistic effective core potential and LANL08(f) uncontracted triple-ζ-valence basis set was initially used for the Re atom [33] in conjunction with the 6-31++G(d, p) double-ζ-split-valence basis set [34,35] for all other atoms, which has been used elsewhere to successfully characterize similar rhenium complexes [36,37]. All computations employed a pruned numerical integration grid with 99 radial shells and 590 angular points per shell and the default threshold of 1×10^{-6} for removing linearly dependent basis functions. Orbital images were prepared with Avogadro 1.0.3 with an iso value of 0.25.

3.2. Electron Lifetime Measurement Information

All sample concentrations were on the order of 10^{-5} M to reduce reabsorption. Luminescence lifetimes were obtained by exciting with the 485 nm line of a pulsed diode laser (fwhm < 100 ps) and detecting with a PicoQuant PDM series single photon avalanche diode (Micro Photon Devices, Bolzano, Italy).

3.3. Photocatalysis General Information

Prior to experimentation, glassware was flame-dried under vacuum, then kept under nitrogen pressure. MeCN was dried for 24 h over calcium hydride, distilled with the first and last 20% of the solvent discarded, and stored under nitrogen with dry 3 Å molecular sieves prior to being used as the solvent source. Solvent, triethylamine, and catalyst solutions were added via dry, nitrogen-flushed syringes. Photosensitizer solutions were prepared in flame-dried 10 mL round-bottom flasks. BIH was added under positive nitrogen pressure.

Irradiation for photocatalytic experiments was performed with a 150W Sciencetech SF-150C Small Collimated Beam Solar Simulator equipped with an AM1.5 filter (Sciencetech, London, ON, Canada). Headspace analysis was performed using a gastight syringe with stopcock and Agilent 7890B Gas Chromatograph (column, Agilent PorapakQ 6 ft, 1/8 OD) (Agilent, Santa Clara, CA, USA). Quantitations of CO and CH$_4$ were made using an FID, while H$_2$ was quantified using a TCD (all calibrated using standards purchased from BuyCalGas.com) (Cross Company, Greensboro, NC, USA).

3.4. Water-Control Photocatalysis Procedure

To a flame-dried 17 mL flask were added BIH (0.005 g, 0.02 mmol), dry MeCN (1.8 mL), and catalyst (0.2 mL of a 1 × 10^{-3} M in dry MeCN solution). H_2O was added via a microsyringe. The solution was then bubbled vigorously for at least 15 min, until the total volume reached 1.9 mL. At that time, degassed, dry triethylamine (0.1 mL) was added to the sealed flask by syringe. The samples were then irradiated with a solar simulator (150 W Xe lamp, AM1.5 filter).

3.5. Oxygen Control Photocatalysis Procedure

To a flame-dried 17 mL flask were added BIH (0.005 g, 0.02 mmol), dry MeCN (1.8 mL), and catalyst (0.2 mL of a 1× 10^{-3} M in dry MeCN solution)A quantity of 4µL of H_2O (0.2% *v*/*v*) was added via a 10 µL microsyringe. The solution was then bubbled vigorously for at least 15 min, until the total volume reached 1.9 mL. At that time, degassed, dry triethylamine (0.1 mL) was added to the sealed flask by syringe. Using a gastight syringe with stopcock, CO_2 was removed and replaced with a % *v*/*v* ambient atmosphere. The samples were then irradiated with a solar simulator (150 W Xe lamp, AM1.5 filter).

Supplementary Materials: Supplementary materials can be found at www.mdpi.com/2304-6740/6/1/22/s1: Cartesian coordinates for the geometry optimizations of Re(pyNHC-PhCF_3)(CO)$_3$Br as both the neutral and anionic complex.

Acknowledgments: Casey A. Carpenter, Phillip Brogdon, Louis E. Mcnamara, Nathan I. Hammer, and Jared H. Delcamp thank NSF award OIA-1539035. Gregory S. Tschumper thanks NSF awards OIA-1430364 and CHE-1664998.

Author Contributions: All authors conceived and designed the experiments; Casey A. Carpenter and Phillip Brogdon performed the photocatalysis experiments; Louis E. Mcnamara performed the TCSPC experiments; Gregory S. Tschumper performed the computations; Casey A. Carpenter, Phillip Brogdon and Jared H. Delcamp analyzed the photocatalysis data; Louis E. Mcnamara and Nathan I. Hammer analyzed the TCSPC data; Gregory S. Tschumper and Jared H. Delcamp analyzed the computational data; Nathan I. Hammer, Gregory S. Tschumper, and Jared H. Delcamp contributed reagents/materials/instrument access; Jared H. Delcamp wrote the paper.

Conflicts of Interest: The authors declare no conflict of interest.

References

1. **Robert, M. Running the clock. CO_2 catalysis in the age of anthropocene. *ACS Energy Lett.* 2016, 281–282. [CrossRef]**
2. **Appel, A.M.; Bercaw, J.E.; Bocarsly, A.B.; Dobbek, H.; DuBois, D.L.; Dupuis, M.; Ferry, J.G.; Fujita, E.; Hille, R.; Kenis, P.J.; et al. Frontiers, opportunities, and challenges in biochemical and chemical catalysis of CO_2 fixation. *Chem. Rev.* 2013, *113*, 6621–6658. [CrossRef] [PubMed]**
3. **Hammer, N.I.; Sutton, S.; Delcamp, J.H.; Graham, J.D. Photocatalytic water splitting and carbon dioxide reduction. In *Handbook of Climate Change Mitigation and Adaptation*; Chen, W.-Y., Suzuki, T., Lackner, M., Eds.; Springer: New York, NY, USA, 2016; pp. 2709–2756.**
4. **Berardi, S.; Drouet, S.; Francas, L.; Gimbert-Surinach, C.; Guttentag, M.; Richmond, C.; Stoll, T.; Llobet, A. Molecular artificial photosynthesis. *Chem. Soc. Rev.* 2014, *43*, 7501–7519. [CrossRef] [PubMed]**
5. **Benson, E.E.; Kubiak, C.P.; Sathrum, A.J.; Smieja, J.M. Electrocatalytic and homogeneous approaches to conversion of CO_2 to liquid fuels. *Chem. Soc. Rev.* 2009, *38*, 89–99. [CrossRef] [PubMed]**
6. **Morris, A.J.; Meyer, G.J.; Fujita, E. Molecular approaches to the photocatalytic reduction of carbon dioxide for solar fuels. *Acc. Chem. Res.* 2009, *42*, 1983–1994. [CrossRef] [PubMed]**
7. **Sato, S.; Morikawa, T.; Kajino, T.; Ishitani, O. A highly efficient mononuclear iridium complex photocatalyst for CO_2 reduction under visible light. *Angew. Chem. Int. Ed.* 2013, *52*, 988–992. [CrossRef] [PubMed]**
8. **Sato, S.; Morikawa, T. [Ir(tpy)(bpy)Cl] as a photocatalyst for CO_2 reduction under visible-light irradiation. *ChemPhotoChem* 2017. [CrossRef]**
9. **Hawecker, J.; Lehn, J.-M.; Ziessel, R. Efficient photochemical reduction of CO_2 to CO by visible light irradiation of systems containing Re(bipy)(CO)$_3$X or Ru(bipy)$_3^{2+}$–Co^{2+} combinations as homogeneous catalysts. *J. Chem. Soc. Chem. Commun.* 1983, 536–538. [CrossRef]**

10. **Huckaba, A.J.; Sharpe, E.A.; Delcamp, J.H. Photocatalytic reduction of CO_2 with Re–pyridyl–NHCs.** *Inorg. Chem.* **2016**, *55*, **682–690.** [CrossRef] [PubMed]
11. **Sahara, G.; Ishitani, O. Efficient photocatalysts for CO_2 reduction.** *Inorg. Chem.* **2015**, *54*, **5096–5104.** [CrossRef] [PubMed]
12. **Rao, H.; Bonin, J.; Robert, M. Non-sensitized selective photochemical reduction of CO_2 to CO under visible light with an iron molecular catalyst.** *Chem. Commun.* **2017**, *53*, **2830–2833.** [CrossRef] [PubMed]
13. **Liyanage, N.P.; Dulaney, H.A.; Huckaba, A.J.; Jurss, J.W.; Delcamp, J.H. Electrocatalytic reduction of CO_2 to CO with Re-pyridyl-NHCs: Proton source influence on rates and product selectivities.** *Inorg. Chem.* **2016**, *55*, **6085–6094.** [CrossRef] [PubMed]
14. **Cope, J.D.; Liyanage, N.P.; Kelley, P.J.; Denny, J.A.; Valente, E.J.; Webster, C.E.; Delcamp, J.H.; Hollis, T.K. Electrocatalytic reduction of CO_2 with CCC-NHC pincer nickel complexes.** *Chem. Commun.* **2017**, *53*, **9442–9445.** [CrossRef] [PubMed]
15. **Agarwal, J.; Shaw, T.W.; Stanton, C.J., 3rd; Majetich, G.F.; Bocarsly, A.B.; Schaefer, H.F., 3rd. NHC-containing manganese(I) electrocatalysts for the two-electron reduction of CO_2.** *Angew. Chem. Int. Ed.* **2014**, *53*, **5152–5155.** [CrossRef]
16. **Jin, T.; He, D.; Li, W.; Stanton, C.J.; Pantovich, S.A.; Majetich, G.F.; Schaefer, H.F.; Agarwal, J.; Wang, D.; Li, G. CO_2 reduction with Re(I)–NHC compounds: Driving selective catalysis with a silicon nanowire photoelectrode.** *Chem. Commun.* **2016**, *52*, **14258–14261.** [CrossRef] [PubMed]
17. **Stanton, C.J., 3rd; Machan, C.W.; Vandezande, J.E.; Jin, T.; Majetich, G.F.; Schaefer, H.F., 3rd; Kubiak, C.P.; Li, G.; Agarwal, J. Re(I)NHC complexes for electrocatalytic conversion of CO_2.** *Inorg. Chem.* **2016**, *55*, **3136–3144.** [CrossRef] [PubMed]
18. **Stanton, C.J., 3rd; Vandezande, J.E.; Majetich, G.F.; Schaefer, H.F., 3rd; Agarwal, J. Mn–NHC electrocatalysts: Increasing π-acidity lowers the reduction potential and increases the turnover frequency for CO_2 reduction.** *Inorg. Chem.* **2016**, *55*, **9509–9512.** [CrossRef] [PubMed]
19. **Boudreaux, C.M.; Liyanage, N.P.; Shirley, H.; Siek, S.; Gerlach, D.L.; Qu, F.; Delcamp, J.H.; Papish, E.T. Ruthenium(II) complexes of pyridinol and N-heterocyclic carbene derived pincers as robust catalysts for selective carbon dioxide reduction.** *Chem. Commun.* **2017**, *53*, **11217–11220.** [CrossRef] [PubMed]
20. **Hopkinson, M.N.; Richter, C.; Schedler, M.; Glorius, F. An overview of N-heterocyclic carbenes.** *Nature* **2014**, *510*, **485–496.** [CrossRef] [PubMed]
21. **Kelly, R.A., III; Clavier, H.; Giudice, S.; Scott, N.M.; Stevens, E.D.; Bordner, J.; Samardjiev, I.; Hoff, C.D.; Cavallo, L.; Nolan, S.P. Determination of N-heterocyclic carbene (NHC) steric and electronic parameters using the [(NHC)Ir(CO)$_2$Cl] system.** *Organometallics* **2008**, *27*, **202–210.** [CrossRef]
22. **Feroci, M.; Chiarotto, I.; Inesi, A. Advances in the knowledge of N-heterocyclic carbenes properties. The backing of the electrochemical investigation.** *Catalysts* **2016**, *6*, **178.** [CrossRef]
23. **Cavallo, L.; Correa, A.; Costabile, C.; Jacobsen, H. Steric and electronic effects in the bonding of N-heterocyclic ligands to transition metals.** *J. Organomet. Chem.* **2005**, *690*, **5407–5413.** [CrossRef]
24. **Takeda, H.; Koike, K.; Inoue, H.; Ishitani, O. Development of an Efficient Photocatalytic System for CO2 Reduction Using Rhenium(I) Complexes Based on Mechanistic Studies** *J. Am. Chem. Soc.* **2008**, *130*, **2023–2031.** [CrossRef] [PubMed]
25. **Mukuta, T.; Simpson, P.V.; Vaughan, J.G.; Skelton, B.W.; Stagni, S.; Massi, M.; Koike, K.; Ishitani, O.; Onda, K. Photochemical processes in a rhenium(I) tricarbonyl N-heterocyclic carbene complex studied by time-resolved measurements.** *Inorg. Chem.* **2017**, *56*, **3404–3413.** [CrossRef] [PubMed]
26. **Vaughan, J.G.; Reid, B.L.; Wright, P.J.; Ramchandani, S.; Skelton, B.W.; Raiteri, P.; Muzzioli, S.; Brown, D.H.; Stagni, S.; Massi, M. Photophysical and photochemical trends in tricarbonyl rhenium(I) N-heterocyclic carbene complexes.** *Inorg. Chem.* **2014**, *53*, **3629–3641.** [CrossRef] [PubMed]
27. **Vaughan, J.G.; Reid, B.L.; Ramchandani, S.; Wright, P.J.; Muzzioli, S.; Skelton, B.W.; Raiteri, P.; Brown, D.H.; Stagni, S.; Massi, M. The photochemistry of rhenium(I) tricarbonyl N-heterocyclic carbene complexes.** *Dalton Trans.* **2013**, *42*, **14100–14114.** [CrossRef] [PubMed]
28. **Feldt, S.M.; Lohse, P.W.; Kessler, F.; Nazeeruddin, M.K.; Grätzel, M.; Boschloo, G.; Hagfeldt, A. Regeneration and recombination kinetics in cobalt polypyridine based dye-sensitized solar cells, explained using Marcus theory.** *Phys. Chem. Chem. Phys.* **2013**, *15*, **7087–7097.** [CrossRef] [PubMed]
29. **Last, G.V.; Schmick, M.T. A review of major non-power-related carbon dioxide stream compositions.** *Environ. Earth Sci.* **2015**, *74*, **1189–1198.** [CrossRef]

30. **Nakajima, T.; Tamaki, Y.; Ueno, K.; Kato, E.; Nishikawa, T.; Ohkubo, K.; Yamazaki, Y.; Morimoto, T.; Ishitani, O. Photocatalytic reduction of low concentration of CO_2. *J. Am. Chem. Soc.* 2016, *138*, 13818–13821. [CrossRef] [PubMed]**
31. **Zhao, Y.; Truhlar, D.G. A new local density functional for main-group thermochemistry, transition metal bonding, thermochemical kinetics, and noncovalent interactions. *J. Chem. Phys.* 2006, *125*, 194101. [CrossRef] [PubMed]**
32. **Frisch, M.J.; Trucks, G.W.; Schlegel, H.B.; Scurseria, G.E.; Robb, M.A.; Cheeseman, J.R.; Scalmani, G.; Barone, V.; Mennucci, B.; Petersson, A.; et al. *Gaussian09*; revision E.01; Gaussian, Inc.: Wallingford, CT, USA, 2009.**
33. **Hay, P.J.; Wadt, W.R. Ab initio effective core potentials for molecular calculations. Potentials for the transition metal atoms Sc to Hg. *J. Chem. Phys.* 1985, *82*, 270–283. [CrossRef]**
34. **Dill, J.D.; Pople, J.A. Self-consistent molecular orbital methods. XV. Extended gaussian-type basis sets for lithium, beryllium, and boron. *J. Chem. Phys.* 1975, *62*, 2921–2923. [CrossRef]**
35. **Francl, M.M.; Pietro, W.J.; Hehre, W.J.; Binkley, J.S.; Gordon, M.S.; DeFrees, D.J.; Pople, J.A. Self-consistent molecular orbital methods. XXIII. A polarization-type basis set for second-row elements. *J. Chem. Phys.* 1982, *77*, 3654–3665. [CrossRef]**
36. **Agarwal, J.; Johnson, R.P.; Li, G. Reduction of CO_2 on a tricarbonyl rhenium(I) complex: Modeling a catalytic cycle. *J. Phys. Chem. A* 2011, *115*, 2877–2881. [CrossRef] [PubMed]**
37. **Agarwal, J.; Fujita, E.; Schaefer, H.F., 3rd; Muckerman, J.T. Mechanisms for CO production from CO_2 using reduced rhenium tricarbonyl catalysts. *J. Am. Chem. Soc.* 2012, *134*, 5180–5186. [CrossRef] [PubMed]**